Oxidation of the Non-Heme Iron Complex in Photosystem II†

Hiroshi Ishikita and Ernst-Walter Knapp*

Institute of Chemistry and Biochemistry, Department of Biology, Chemistry, and Pharmacy, Free University of Berlin, Takustrasse 6, D-14195 Berlin, Germany

Received June 9, 2005; Revised Manuscript Received August 13, 2005

ABSTRACT: In photosystem II (PSII), the redox properties of the non-heme iron complex (Fe complex) are sensitive to the redox state of quinones ($Q_{A/B}$), which may relate to the electron/proton transfer. We calculated the redox potentials for one-electron oxidation of the Fe complex in PSII [E_m(Fe)] based on the reference value E_m(Fe) = +400 mV at pH 7 in the $Q_A^0Q_B^0$ state, considering the protein environment in atomic detail and the associated changes in protonation pattern. Our model yields the pH dependence of E_m(Fe) with −60 mV/pH as observed in experimental redox titration. We observed significant deprotonation at D1-Glu244 in the hydrophilic loop region upon Fe complex oxidation. The calculated pK_a value for D1-Glu244 depends on the Fe complex redox state, yielding a pK_a of 7.5 and 5.5 for Fe^{2+} and Fe^{3+}, respectively. To account for the pH dependence of E_m(Fe), a model involving not only D1-Glu244 but also the other titratable residues (five Glu in the D-*de* loops and six basic residues near the Fe complex) seems to be needed, implying the existence of a network of residues serving as an internal proton reservoir. Reduction of $Q_{A/B}$ yields +302 mV and +268 mV for E_m(Fe) in the $Q_A^-Q_B^0$ and $Q_A^0Q_B^-$ states, respectively. Upon formation of the $Q_A^0Q_B^-$ state, D1-His252 becomes protonated. Forming $Fe^{3+}Q_BH_2$ by a proton-coupled electron transfer process from the initial state $Fe^{2+}Q_B^-$ results in deprotonation of D1-His252. The two EPR signals observed at $g = 1.82$ and $g = 1.9$ in the $Fe^{2+}Q_A^-$ state of PSII may be attributed to D1-His252 with variable and fixed protonation, respectively.

The photosynthetic reaction in photosystem II (PSII)[1] is initialized by light absorption. The resulting electronic excitation energy is ultimately converted to chemical potential starting with a charge separation process at the P680 Chl*a* of the D1/D2 proteins. These Chl*a* form an oxidized positively charged $P680^+$, while the released electron travels along the electron transfer (ET) chain. ET is terminated by the two plastoquinones, Q_A and Q_B, at the stromal side. Q_B is released from its binding site to the bulk quinone pool associated with the thylakoidal membrane after double reduction and protonation. A non-heme iron complex (Fe complex) is situated equidistantly from both Q_A and Q_B (Figure 1). Two symmetrical pairs of histidines, D1-His215/D2-His214 and D1-His272/D2-His268, are ligands of the Fe complex, and the two histidines of the former pair form an H bond with Q_B/Q_A, respectively. In addition, the Fe complex has one bicarbonate as a nonprotein ligand. Despite a large degree of structural similarity between PSII and bacterial photosynthetic reaction centers (bRC) (*1*), the bicarbonate is absent in the latter. Instead, in bRC Glu is ligated to the Fe complex. The replacement of Fe^{2+} with Zn^{2+} did not prevent ET between Q_A and Q_B in bRC, and it was formerly suggested that the Fe complex is not a functional redox group (*2*). On the other hand, recent FTIR studies suggested the presence of a yet unknown electron donor to Q_B instead of

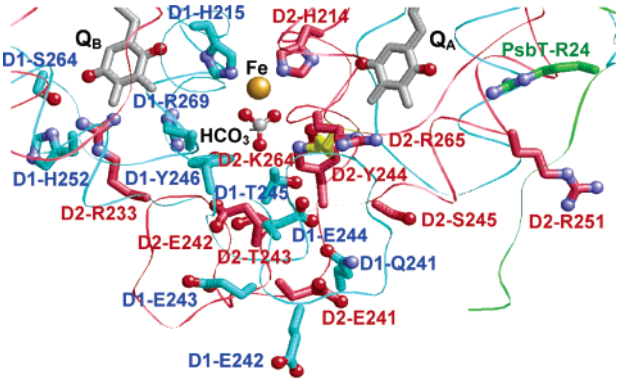

FIGURE 1: Residues in the neighborhood of the Fe complex in PSII. D1, D2, and PsbT are colored in cyan, pink, and green, respectively. For clarity, D2-Lys264 is colored in yellow. The two histidine ligands D1-His272 and D2-His268 above and below the drawing plane are not shown.

† This work was supported by the Deutsche Forschungsgemeinschaft SFB 498, Project A5, and Forschergruppe Project KN 329/5-1/5-2, GRK 80/2, GRK 268, and GRK 788/1. H.I. was supported by the DAAD.

* Corresponding author. Tel: (+49) 30-83854387. Fax: (+49) 30-83856921. E-mail: knapp@chemie.fu-berlin.de.

[1] Abbreviations: BBY-PSII samples, thylakoid fragments of PSII from spinach prepared by detergent treatment according to Berthold et al. (*16*); bicarbonate-in(ex) model, Fe complex model with bicarbonate as the internal component (external titratable group); bRC, bacterial photosynthetic reaction center; Chl*a*, chlorophyll *a*; DCMU, 3-(3,4-dichlorophenyl)-1,1-dimethylurea; DINOSEB, 2-(1-methylpropyl)-4,6-dinitrophenol; D-*de* loop, hydrophilic loop in D1/D2 that connects transmembrane helix D with parallel helix *de*; E_{solv}, solvent redox potential; E_m(Fe), (midpoint) redox potential of the Fe complex for one-electron oxidation (Fe^{2+}/Fe^{3+}); ET, electron transfer; Fe complex, the non-heme iron complex in PSII; LPB equation, linearized Poisson−Boltzmann equation; Mn cluster, oxygen-evolving complex with Mn ions; NHE, normal hydrogen electrode; P680, Chl*a* of PSII related to absorption at 680 nm; pK_a(bias), pK_a calculated as a function of the bias energy at a fixed pH; pK_a(effective), pK_a calculated from the protonation pattern of all titratable residues as a function of solvent pH for a large pH range; PSII, photosystem II; $Q_{A(B)}$, plastoquinone in A(B) branch.

10.1021/bi051099v CCC: $30.25
Published on Web 10/21/2005

Q_A^-, which might be the Fe complex (*3*). Indeed, a reaction mechanism involving the Fe complex in the ET from Q_A^- to Q_B was proposed earlier by Petrouleas and Diner for PSII (*4*).

The role of the bicarbonate at the Fe complex in PSII is a matter of debate. Formerly, a number of research groups proposed that the bicarbonate may be directly involved in the proton transfer event coupled to ET from Q_A to Q_B (*5*, *6*). On the other hand, kinetic studies of Koulougliotis et al. (*7*) revealed no change in the ET rate displacing the bicarbonate by cyanide, suggesting its more indirect role. With redox titration, the redox potential of the Fe complex for one-electron oxidation [E_m(Fe)] was determined to be +400 mV versus NHE at pH 7.0 (*8*, *9*). Despite its redox activity, the Fe complex is unlikely to be relevant in the functional ET process in PSII, since E_m(Fe) is too high with respect to $E_m(Q_{A/B})$ (reviewed in ref *10*). It was also demonstrated in EPR studies (*11*, *12*) that, only after replacement of native Q_B with a high-potential quinone, the Fe complex can be oxidized by Q_B. Nevertheless, the sensitivity of the Fe complex on EPR signals enables this complex to serve as a probe for the $Q_{A/B}$ redox state, which elucidated many details of related reactions. The pH dependence of E_m(Fe) with −60 mV/pH is a strong indication that titratable groups in the neighborhood of the Fe complex deprotonate upon oxidation of the Fe complex (*4*, *8*, *9*). The bicarbonate might be a factor responsible for this pH dependence, but FTIR studies suggested that the bicarbonate ligand does not deprotonate upon oxidation of the Fe complex (*13*). Alternatively, the bicarbonate may influence the pK_a of nearby titratable residues, and these induced changes in the protonation pattern of PSII may affect the redox properties of the Fe complex (*14*).

The crystal structure of PSII isolated from the thermophilic cyanobacterium *Thermosynechococcus elongatus* (*T. elongatus*) revealed details of the protein environment of the Fe complex and the bicarbonate binding site (*15*). A discrepancy of EPR signals for the Fe complex was reported between the standard PSII from cyanobacteria and BBY-PSII samples [thylakoid fragments of PSII from spinach prepared by detergent treatment according to Berthold et al. (*16*)], which is possibly due to the higher Q_B binding affinity in standard PSII (*12*, *17*). On the other hand, recent FTIR difference spectra for $Q_{A/B}$ showed close similarities among the PSII core complex from *T. elongatus*, *Synechocystis* PCC6803, and BBY-PSII (i.e., from spinach), implying their structural similarities (*18*). Thus, the PSII crystal structure from *T. elongatus* is, currently, an appropriate model system to investigate the interaction of the redox states of $Q_{A/B}$ and of the Fe complex in PSII.

In the present study, we titrate the Fe complex and titratable residues in the whole PSII complex. By solving the linearized Poisson−Boltzmann (LPB) equation, we consider all amino acids, redox-active cofactors, and their different charge states. As suggested previously from the crystal structure of bRC (*19*), the specific position of the Fe complex in the vicinity of the hydrophilic loops that connect the transmembrane helix D with helix *de* (D-*de* loop) parallel to the membrane plane in the D1/D2 proteins is of great interest. In the light-induced degradation process of the D1 protein, the D-*de* loop was proposed to be the first target for cleavage of the D1 protein under strong illumination (*20*). The corresponding loop is absent in bRC. The D-*de* loop in PSII is rich in titratable and polar residues. Such a cluster of strongly interacting titratable residues often hinders exact assignment of an apparent pK_a to a specific residue (for instance, those in the proton transfer pathways of bRC; discussed in refs *21* and *22*). In the present computational study, it is possible to focus on an individual titratable residue separately, even for a strongly coupled cluster of residues. Thus, our computational analysis of this region of the D1 protein may provide a clue to understanding deprotonation of titratable residues upon oxidation of the Fe complex in PSII.

COMPUTATIONAL PROCEDURES

Coordinates. In our computations, atomic coordinates were taken from the crystal structure of PSII from thermophilic cyanobacterium *T. elongatus* at 3.5 Å resolution (PDB code 1S5L) (*15*). Hydrogen atoms were generated and energetically optimized with CHARMM (*23*), while the positions of all non-hydrogen atoms were fixed and all titratable groups were kept in their standard protonation states, i.e., acidic groups ionized and basic groups (including titratable histidines) protonated. Simultaneously, Chl*a*, Pheo*a*, and $Q_{A/B}$ were kept in the neutral charge redox states, and the Fe complex was kept in the reduced state with Fe^{2+}. Histidines that are ligands of Chl*a* were treated as nontitratable with neutral total charge.

Atomic Partial Charges. Atomic partial charges of the amino acids were adopted from the all-atom CHARMM22 (*24*) parameter set. The charges of protonated acidic oxygens were both increased symmetrically by +0.5 unit charges to account implicitly for the presence of a proton. Similarly, instead of removing a proton in the deprotonated state, the charges of all protons of the basic groups of arginine and lysine were diminished symmetrically by a total unit charge. For residues whose protonation states are not available in the CHARMM22 parameter set, appropriate charges were computed (*25*). For the cofactors, the same atomic charges as in the previous computation of PSII (*26*−*28*) were used. The atomic charges of the high-spin Fe complex (non-heme iron, one bicarbonate, and protein residues D1-His215/D2-His214 and D1-His272/D2-His268) were determined from the electronic wave functions by fitting the resulting electrostatic potential in the neighborhood of these molecules by the RESP procedure (Supporting Information, Table S1) (*29*). The electronic wave functions were calculated with the DFT module in JAGUAR (*30*) using the B3LYP functional with LACVP basis set (6-31G with effective core potentials on heavy atoms).

Mn Cluster. The Mn cluster is proposed to change its oxidation state from [Mn_4] (II, III, IV_2) in state S_0 via [Mn_4] (III_2, IV_2) in S_1 to [Mn_4] (III, IV_3) in states S_2 and S_3 (*31*). All computations were done in the S_0 state of the Mn cluster. On the basis of the 3.5 Å crystal structure (*15*), we considered the four explicitly given μ-oxo oxygen atoms as O^{2-}, assigned to each Mn ion a charge of +3.25 corresponding to the S_0 state, and included the Ca^{2+} ion and a bicarbonate that is attached to the Mn cluster, resulting in a total positive charge of +6; i.e., the structural model of the Mn cluster is based on ref *15* and the used charges are given in ref *26*.

Computation of Protonation Pattern and Redox Potentials. Our computation is based on the electrostatic continuum

model by solving the LPB equation with the program MEAD (*32*). The protonation patterns were sampled by a Monte Carlo (MC) method with our own program Karlsberg (*33*). The dielectric constant was set to $\epsilon_P = 4$ inside the protein and $\epsilon_W = 80$ for water as done in previous computations (*26*−*28*). All computations refer to 300 K and an ionic strength of 100 mM. The LPB equation was solved using a three-step grid-focusing procedure with 2.5, 1.0, and 0.3 Å resolution. The MC sampling yields the probabilities $[A_{ox}]$ and $[A_{red}]$ for the redox states (or $[A_{protonated}]$ and $[A_{deprotonated}]$ for the protonation states) of compound A. The E_m(Fe) are calculated from the Nernst equation. To minimize the statistical error in evaluating the E_m, a bias potential is applied to obtain an equal amount of both redox states ($[A_{ox}] = [A_{red}]$), yielding the value of the bias potential as the resulting E_m. For convenience, the computed E_m are given with millivolt accuracy, without implying that the last digit is significant.

We calculated pK_a values for titratable residues using two different pK_a definitions. A straightforward approach is that a titratable residue is biased by an individual energy term to be 50% protonated, while the protonation states of the other titratable residues are fully relaxed at a fixed pH (pH 7 in the present study). This bias energy can be used to define the pK_a of this residue [pK_a(bias)]. This pK_a describes how much energy is needed to change the protonation state of this residue in its protein environment where the protonation pattern changes locally by equilibration due to the charge change of this residue without involving changes of solvent pH. This pK_a definition can be useful to describe the energetics of proton transfer processes between different titratable groups. The protonation dependence of the considered titratable residue obeys the Henderson−Hasselbalch equation (equivalent to the Nernst equation for a redox-active group) as a function of the bias energy.

Another approach to determine pK_a values is to calculate it from the protonation pattern of all titratable residues as a function of solvent pH for a large pH interval. Here, the pK_a of the titratable residue under consideration can be defined as the pH value where this residue is to 50% protonated [pK_a(effective)]. This is a more common pK_a definition and corresponds to the conditions where pK_a values of titratable groups in proteins can be determined experimentally. When the molecular system contains only a single titratable group or several noninteracting titratable groups, the same pK_a values are computed for both definitions, the same pK_a value is computed for both definitions with [pK_a(bias)] and [pK_a(effective)]. For further information about computational procedures and error estimate, see previous work for E_m (*26*) and pK_a (*34*).

Influence of Ionic Strength on E_m(Fe). We uniformly used the ionic strength of 100 mM for computations of PSII as done for other systems. The ionic strength has a tendency to screen the influence of atomic charges on the protein surface. Large ionic strength diminishes the influence of surface atomic charges. To evaluate the *direct* influence of the ionic strength, we calculated E_m(Fe) with the ionic strength of 0 and 100 mM, fixing the protonation state of the titratable residues to standard protonation (i.e., deprotonated acidic and protonated basic residues). As a consequence, the ionic strength of 100 mM downshifts E_m(Fe) by 78 mV relative to 0 mM (based on the bicarbonate-in model, described later), indicating that the ionic strength stabilizes the oxidized state of the Fe complex. However, when we consider the equilibrium protonation pattern of all titratable groups in PSII, the increase in ionic strength from 0 to 100 mM results in a difference of only 4 mV in the calculated E_m(Fe). The resulting tiny difference in E_m(Fe) is due to compensation effects by small changes in protonation of several residues in response to the change in ionic strength, implying a buffering effect of titratable residues. Therefore, unless the redox-active group is on the protein surface and simultaneously isolated from other titratable residues, its E_m remains essentially unchanged in the presence of a sufficient amount of titratable residues.

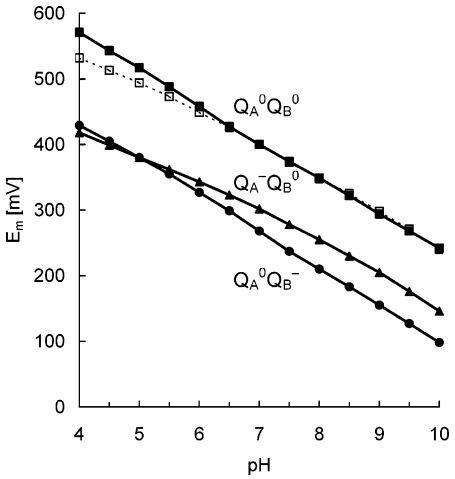

FIGURE 2: Calculated pH dependence of E_m(Fe) in PSII. Bicarbonate-in model (bicarbonate is treated as an integral part of the Fe complex): (■) $Q_A^0Q_B^0$; (▲) $Q_A^-Q_B^0$; (●) $Q_A^0Q_B^-$. Bicarbonate-ex model (bicarbonate is treated as a molecular group independent from the Fe complex): (□) $Q_A^0Q_B^0$.

RESULTS

Reference Model System for the Fe Complex in PSII. As a reference model system, we consider a complex with a non-heme iron ligated by a bicarbonate and protein residues, D1-His215/D2-His214 and D1-His272/D2-His268 (bicarbonate-in model). This complex can be modeled as a tetraimidazole iron with a carboxylic acid. However, the E_m for such a model compound is unknown so far. Thus, we tentatively calculated E_m(Fe) in the protein environment of PSII for the $Q_A^0Q_B^0$ redox state with the LPB equation at pH 7.0 and fitted the obtained value to the measured value of +400 mV (*8*, *9*) for E_m(Fe) in PSII at pH 7.0. Alternatively, another complex that lacks the bicarbonate may be considered as a reference model system, i.e., a complex with a non-heme iron ligated only by the protein residues D1-His215/D2-His214 and D1-His272/D2-His268 (bicarbonate-ex model). In this case, the bicarbonate ligated to the non-heme iron is treated as an external titratable group separated from the Fe complex.

Both reference models yield similar pH dependences of the calculated E_m(Fe) in PSII above pH ∼6.5. A deviation is observed below this pH; the slope remained at −59 mV/pH for E_m(Fe) in the bicarbonate-in model but changed to −45 mV/pH for E_m(Fe) in the bicarbonate-ex model (Figure 2). This discrepancy originates from the latter model due to its less dependent behavior of the bicarbonate from the Fe complex during the titration, which is consistent with its pK_a

value of 6.4. Remarkably, even in the bicarbonate-ex model, the bicarbonate remains ionized over the whole range of the pH investigated. Thus, the discrepancy in the E_m(Fe) pH dependence between the two models cannot be related to a change in bicarbonate protonation but is due to pK_a shifts of other residues nearby that are invoked by the difference in the two models. We found that below pH 6.5 the two models provide different protonation states for D1-Glu244. For instance, at pH 5.5 D1-Glu244 is protonated by 0.53 H^+ in the bicarbonate-in model but protonated by 0.89 H^+ in the bicarbonate-ex model. Indeed, D1-Glu244 is the acidic residue that is most proximal to the bicarbonate binding site in the PSII crystal structure ($O_{bicarbonate}-O_{Glu}$ distance of 5.4 Å) (*15*). Only one residue, D1-Tyr246, placed between the bicarbonate and D1-Glu244 ($O_{bicarbonate}-O_{Tyr}$ distance of 3.2 Å and $O_{Tyr}-O_{Glu}$ distance of 6.9 Å) is closer to the bicarbonate/Fe complex.

From experimental redox titration, it has been established that the pH dependence of E_m(Fe) in PSII exhibits a slope of −60 mV/pH in the pH range of 5.5−8.5 (*4*, *8*, *9*). In the present study, the same pH dependence is seen for the bicarbonate-in model but not for the bicarbonate-ex model. In addition, if the bicarbonate or the reconstituted carboxylate anions ligate to the Fe complex, their charge distribution and protonation state should vary with the Fe complex redox state. A change of their protonation state decoupled from the redox state of the Fe complex is, for energetic reasons, very unlikely. Since in the bicarbonate-in model the atomic partial charges of the Fe complex were calculated with the bicarbonate, our description of the Fe complex with the bicarbonate-in model seems to be more realistic than the one with the bicarbonate-ex model. Indeed, experimental redox titrations revealed that there is little correlation between the pK_a of these reconstituted carboxylate anions and the concomitant pH dependence of E_m(Fe) (*35*). Hence, changes in E_m(Fe) and their pH dependence resulting from bicarbonate replacement are more likely the consequence of altered pK_a of nearby titratable residues (summarized in ref *36*). Therefore, in the following part, we focus on the computational results using the bicarbonate-in model.

pH Dependence of the Protonation Pattern for $Q_A^0Q_B^0$. To compare the pH dependence of the calculated E_m(Fe), we determined the protonation states of titratable residues in PSII for the redox equilibrium of the Fe complex, i.e., $[Fe^{2+}] = [Fe^{3+}]$. In the $Q_A^0Q_B^0$ redox state, D1-Glu244 is protonated by 0.4−0.6 H^+ in the wide pH range of 4.5−8.0 with a remarkably weak pH dependence (Figure 3a), indicating that the pK_a(effective) value for D1-Glu244 is around 4.5−8.0. This is essentially consistent with a pK_a(bias) of 7.5 (5.5) in the Fe^{2+} (Fe^{3+}) state calculated for D1-Glu244 in the present study. Under the same conditions, D1-His252 is protonated by 0.5 H^+ at pH ∼5.5, corresponding to a pK_a(effective) of ∼5.5. At higher pH values the titration curves for these residues are more complicated. At pH ∼8, protonation states of four residues (D1-Glu243, D1-Glu244, D2-Arg265, and PsbT-Arg24) near the Fe complex are simultaneously nearly 0.5 H^+ (Figure 3a). However, a direct influence of D2-Arg265 and PsbT-Arg24 on the oxidation of the Fe complex can be excluded, because the two residues do not change their protonation state at pH ∼8 upon oxidation of the Fe complex (Figure 4a). Instead, a significant proton release is observed from D1-Glu-244 in the wide pH range, partially from D1-His252 at lower pH of 5−6, while proton uptake is observed partially by D1-Glu243 at a higher pH of 7−8 (Figure 4a). Therefore, in the stoichiometry of the protons released, D1-Glu244 is responsible for a proton release by 0.6−0.8 H^+ at pH 5−8.5 in the $Q_A^0Q_B^0$ redox state.

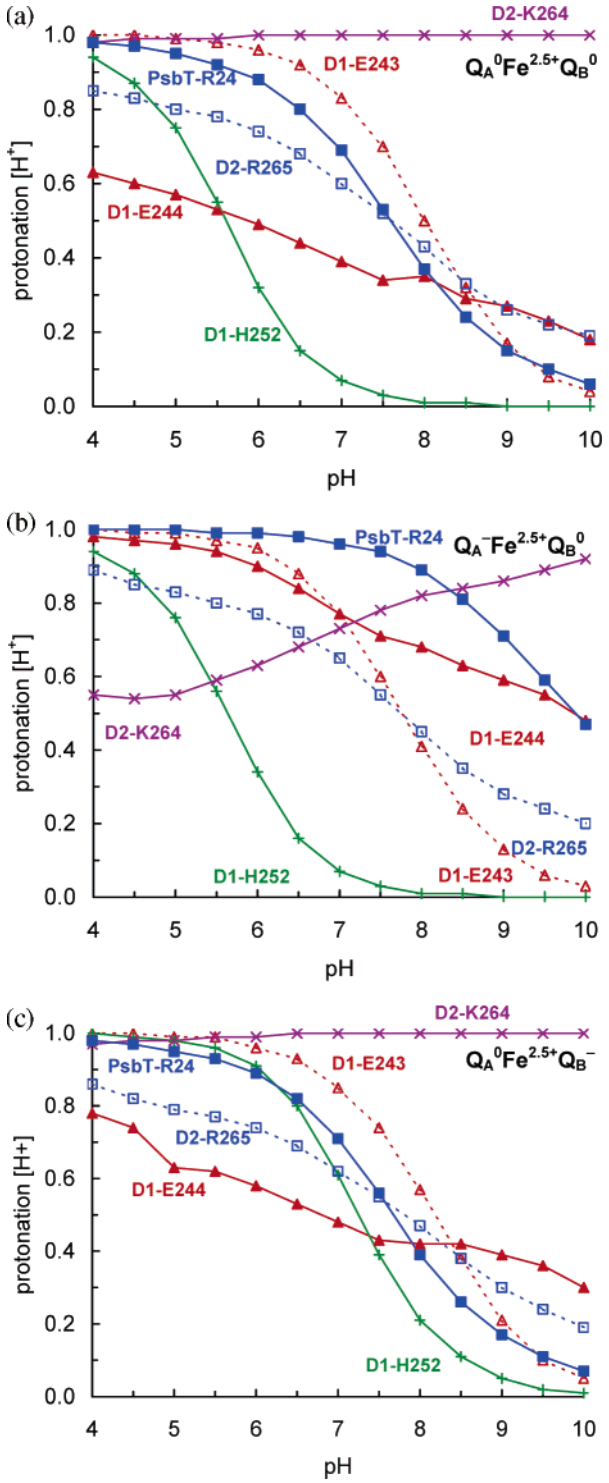

FIGURE 3: pH dependence of PSII protonation states from selected residues with $[Fe^{2+}] = [Fe^{3+}]$: (a) $Q_A^0Q_B^0$, (b) $Q_A^-Q_B^0$, and (c) $Q_A^0Q_B^-$ redox states. Curves: D1-Glu243 (△ in red), D1-Glu244 (▲ in red), D1-His252 (+ in green), D2-Lys264 (× in purple), D2-Arg265 (□ in blue), and PsbT-Arg265 (■ in blue).

The same conclusion is obtained also from computational redox titration to determine the E_m(Fe) by changing the

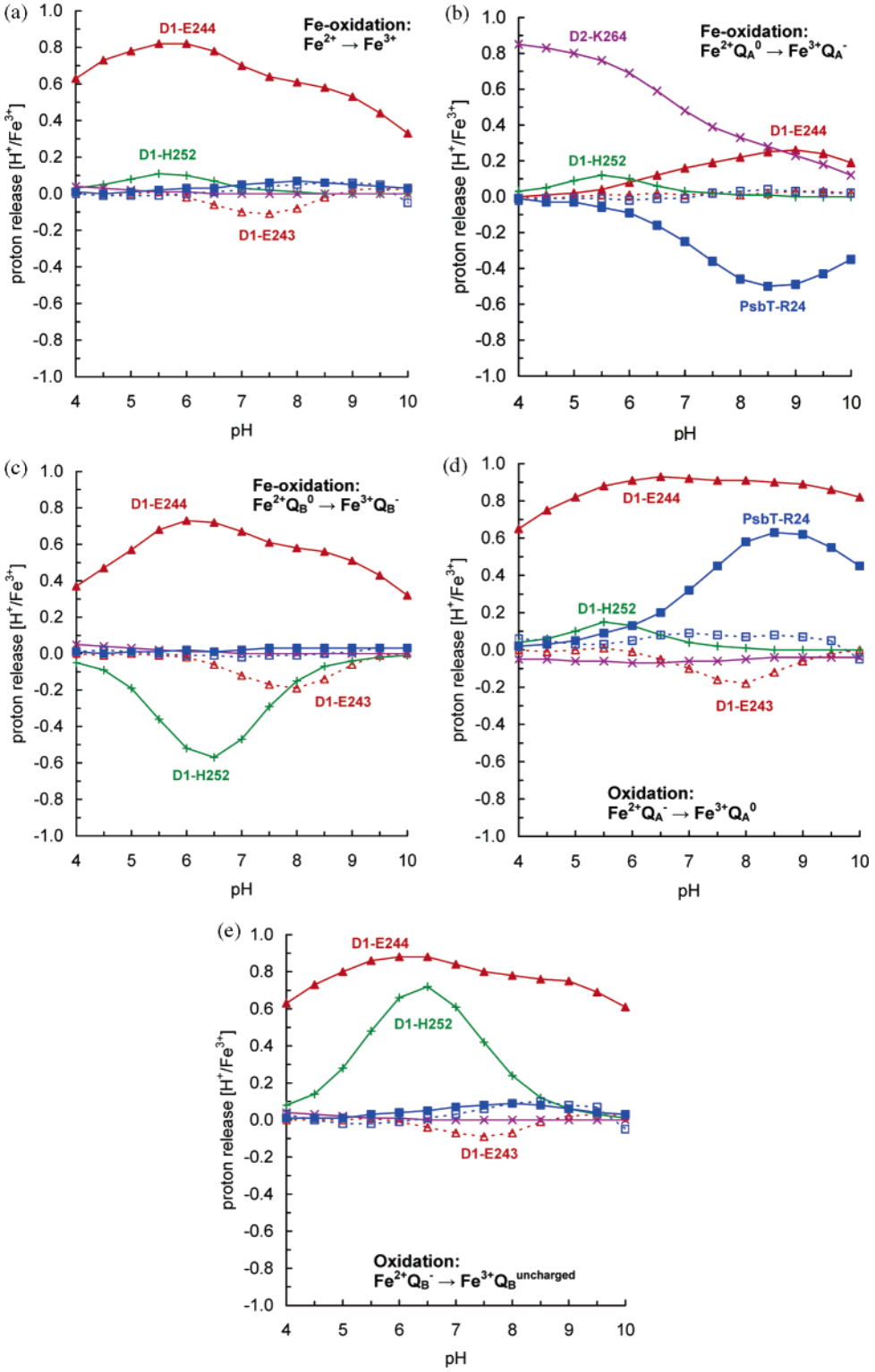

FIGURE 4: pH dependence of PSII proton release upon oxidation of the Fe complex ($Fe^{2+} \rightarrow Fe^{3+}$). The individual influence from dominant titratable residues is shown. Panels: (a) with $Q_A^0Q_B^0$, (b) with $Q_A^-Q_B^0$, (c) with $Q_A^0Q_B^-$, (d) for the transition $Fe^{2+}Q_A^- \rightarrow Fe^{3+}Q_A^0$, and (e) for the transition $Fe^{2+}Q_B^- \rightarrow Fe^{3+}Q_B^{uncharged}$. $Q_B^{uncharged}$ should represent Q_B^0, Q_BH^0, and $Q_BH_2^0$, although the computations were done for the Q_B^0 state only. Curves: D1-Glu243 (△ in red), D1-Glu244 (▲ in red), D1-His252 (+ in green), D2-Lys264 (× in purple), D2-Arg265 (□ in blue), and PsbT-Arg265 (■ in blue).

solvent redox potential (E_{solv}). To compare directly with the experimental results of Petrouleas and Diner (*4*, *35*), we performed the redox titration at pH 6.0 (Figure 5a,c,e) and pH 7.5 (Figure 5b,d,f) for different $Q_{A/B}$ redox states. In the $Q_A^0Q_B^0$ redox state, oxidation of the Fe complex is accompanied by deprotonation of D1-Glu244 and partial deprotonation of D1-His252 at lower pH (6.0) (Figure 5a), while it is accompanied by deprotonation of D1-Glu244 and partial protonation of D1-Glu243 at higher pH (7.5) (Figure 5b).

pH Dependence of the Protonation Pattern in the $Q_A^-Q_B^0$ State. Under the redox equilibrium of the Fe complex in the $Q_A^-Q_B^0$ redox state, the protonation states for D2-Lys264, PsbT-Arg24, and D1-Glu244 shift significantly with respect

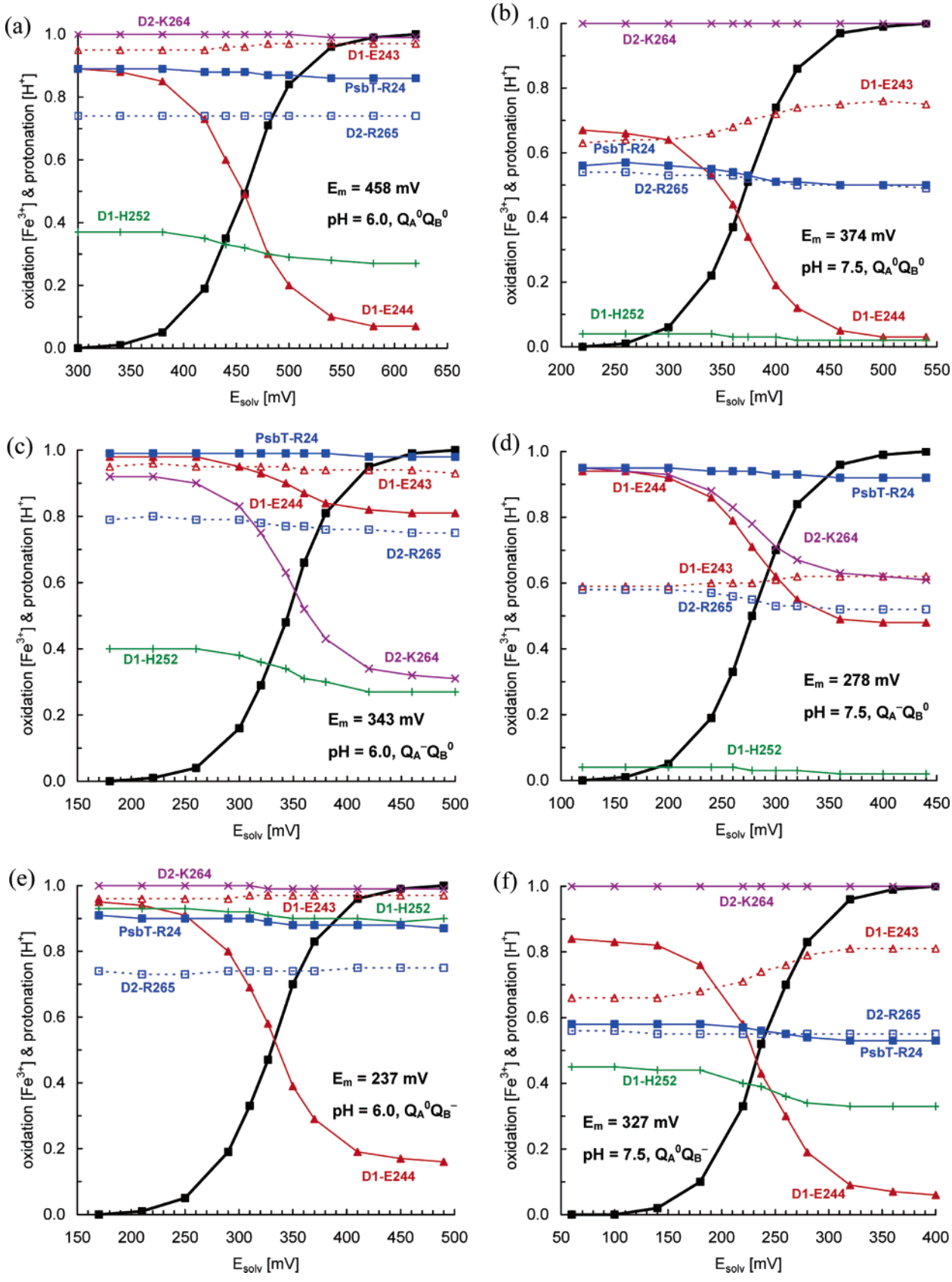

FIGURE 5: Redox titration of the Fe complex in PSII by varying the solvent redox potential E_{solv}. The protonation states for selected titratable residues are displayed as a function of E_{solv} for different charge states of the quinones. Panels: $Q_A^0Q_B^0$ at (a) pH 6.0 and (b) pH 7.5, $Q_A^-Q_B^0$ at (c) pH 6.0 and (d) pH 7.5, and $Q_A^0Q_B^-$ at (e) pH 6.0 and (f) pH 7.5. Curves: (■) redox titration of the Fe complex. The meaning of symbols and colors is the same as in Figures 3 and 4.

to those in the $Q_A^0Q_B^0$ redox state (Figure 3b). Hereby, the pK_a(effective) values can be assigned to be 4−5.5 for D2-Lys264, 10 for PsbT-24, and 9.5−10 for D1-Glu244. At lower pH, proton release occurs mainly from D2-Lys264 (more than 0.7 H^+ below pH 6) upon formation of the $Fe^{3+}Q_A^-$ state (Figure 4b), which is in contrast to the proton release mainly from D1-Glu244 in the $Q_A^0Q_B^0$ redox state (Figure 4a). On the other hand, at higher pH, we observed proton release mainly from both D2-Lys264 and D1-Glu244 (by 0.2−0.3 H^+ at pH 8−9) and proton uptake of PsbT-Arg24 (by 0.5 H^+ at pH 8−9) (Figure 4a). The protonation state of D2-Lys264 is directly coupled to the redox state of the Fe complex at both low (Figure 5c) and high pH (Figure 5d). The protonation states of D1-His252 or D1-Glu244 are less strongly coupled to the redox state of the Fe complex at low pH or both low and high pH, respectively. However, despite the significant proton uptake of PsbT-Arg24 upon formation of the $Fe^{3+}Q_A^-$ state (Figure 4b), the protonation state of this residue remains unchanged in solvent redox titration (E_{solv} change) (Figure 5c,d), suggesting that proton uptake of PsbT-Arg24 is coupled with reduction of Q_A rather than with oxidation of the Fe complex.

pH Dependence of the Protonation Pattern for $Q_A^0Q_B^-$. The pH dependence of the protonation pattern for the $Q_A^0Q_B^-$ redox state (Figure 3c) resembles those for the $Q_A^0Q_B^0$ redox state (Figure 3a) considerably, except for the pK_a(effective) increase of D1-His252 by ∼2 units. This behavior is consistent with a significant proton uptake of D1-His252 by more than 0.4 H^+ at pH 5.5−7.5 upon formation of the $Fe^{3+}Q_B^-$ state (Figure 4c), which is not observed in the other $Q_{A/B}$ redox states. However, the protonation state of D1-His252 is not directly coupled to the redox state of the Fe complex at pH 6.0 (Figure 5e) and only weakly at pH 7.5 (Figure 5f), indicating that its higher pK_a(effective) value and its significant proton uptake in the $Q_A^0Q_B^-$ redox state are due to Q_B reduction rather than Fe complex oxidation.

DISCUSSION

Deprotonation of D1-Glu244 upon Oxidation of the Fe Complex. Upon oxidation of the Fe complex at pH 7 in the $Q_A^0Q_B^0$ redox state, we observed deprotonation of 0.7 H^+ for D1-Glu244 and a small amount of protonation of 0.1 H^+ for D1-Glu243 (Figure 4a). The stronger coupling of D1-Glu244 to the Fe complex may be related to the distances of these residues from the Fe complex ($Fe-O_{Glu}$ distance of 9 Å for D1-Glu244 and 14 Å for D1-Glu243) (Figure 1). Other residues are not significantly affected. Therefore, in the $Q_A^0Q_B^0$ redox state D1-Glu243 and especially D1-Glu244 are the most important residues for the redox reaction of the Fe complex in PSII.

The D-*de* loop of the D1/D2 proteins is located in the region between the Fe complex and the stromal PSII surface (*19*). The corresponding section of the protein sequence is an insertion specific to PSII that is absent in bRC. Both D1-Glu243 and D1-Glu244 are components of the highly conserved five Glu residues (D1−242 to D1−244 and D2−241 to D2−242) in the D-*de* loops (Figure 1). The QEEET motif between D1−241 and D1−245 has, particularly, physiological importance as being the predominant motive for cleavage of the D1 protein. The exact mechanism invoking D1 degradation is unclear, but it becomes necessary under strong illumination with light (*20*), which leads to triplet state accumulation at the Chl*a* in D1 resulting ultimately in harmful singlet oxygen.

Wraight (*9*) observed a pH dependence of E_m(Fe) with a slope of −60 mV/pH and an apparent pK_a value of 8 or 5.3 depending on the Fe complex redox state Fe^{2+} or Fe^{3+}. In the present study, we calculated the pK_a values for titratable residues using the two pK_a definitions, pK_a(bias) and pK_a(effective), introduced in the Computational Procedures section. In the $Q_A^0Q_B^0$ redox state, the calculated pK_a(bias) for D1-Glu244 is dramatically shifted by varying the Fe complex redox state, yielding 7.5 in the Fe^{2+} state and 5.5 in the Fe^{3+} state. This behavior is essentially consistent with a protonation of D1-Glu244 by 0.4−0.6 H^+ in a wide pH range of 4.5−8.0, which is equivalent to pK_a(effective) (Figure 3a). With replacement of the bicarbonate by other small carboxylate anions, Deligiannakis et al. (*35*, *36*) observed changes in E_m(Fe) and its pH dependence and interpreted these altered E_m(Fe) properties as a consequence of pK_a shifts of protein titratable groups by bicarbonate replacement. They also suggested that the same groups were likely responsible for the pH dependence of E_m(Fe).

It is unlikely that the pK_a of the bicarbonate or reconstituted carboxylate anions determines properties of E_m(Fe) directly, since upon replacement of the bicarbonate with carboxylate anions the measured E_m(Fe) and its pH dependence exhibited only small correlations with the pK_a of the reconstituted carboxylate anions (*35*). Even if the reconstituted carboxylate anions have a similar level of pK_a values, their individual molecular structures may require different structural rearrangements of nearby titratable side chains to allow ligation at the Fe complex. Presumably, the pK_a of these residues are shifted due to these structural rearrangements caused by binding of carboxylate anions. In this context, the present computation suggests that D1-Glu244 is likely to be one of those whose pK_a will be significantly affected by bicarbonate replacement with other carboxylate anions, and thus it influences E_m(Fe). Therefore, D1-Glu244 may be the titratable residue discussed by Wraight (*9*) and Deligiannakis et al. (*35*, *36*) (but see discussion later).

Protonation State of D1-Glu243. The protonation change of D1-Glu243 upon oxidation of the Fe complex is small. However, we obtain a pK_a(bias) of 7.6 (7.9) in the Fe^{2+} (Fe^{3+}) state with the $Q_A^0Q_B^0$ redox state. These values are remarkably high with respect to that of 4.4 for glutamic acid in aqueous solution. This is indicative for a negatively charged environment in the neighborhood of D1-Glu243, which is surrounded by D1-Glu242 and D1-Glu244. Astonishingly, D1-Glu243 is solvent exposed, but the proximity of the D2-Pro237 backbone carbonyl oxygen ($O_{Glu}-O_{Pro}$ distance of 4.1 Å) seems to favor the neutral charge state of D1-Glu243. Although mutation of D1-Glu243 to Gln resulted in accelerated D1 protein degradation, the rate of ET from Q_A to Q_B in this mutant did not differ from that of the wild type (*37*). The high pK_a(bias) value for D1-Glu243 in the present study implies that this acidic residue is likely protonated at pH 7, which agrees with the mutational study of Glu243 to Gln (*37*).

The small pK_a(bias) difference for D1-Glu243 in response to the change of the Fe redox state implies that this residue does not relate to the redox properties of the Fe complex

unlike D1-Glu244. Indeed, when the protonation state of D1-Glu243 is constrained (either to ionized or protonated), the pH dependence of E_m(Fe) remains unchanged (for further discussion, see the next section). Furthermore, if the protonation state of D1-Glu243 would be directly coupled to the Fe redox state, it should lead to deprotonation rather than protonation of D1-Glu243. Therefore, the small protonation of D1-Glu243 by 0.1 H^+ upon oxidation of the Fe complex can be attributed to a partial compensation of the induced ionization of D1-Glu244 rather than to a direct influence from the redox change of the Fe complex. Such a coupling of the D1-Glu243 and D1-Glu244 protonation states points to the existence of a network of titratable residues in the neighborhood of the Fe complex (see the next section).

Residues Responsible for the pH Dependence of E_m(Fe). According to former studies on PSII, the pH dependence of E_m(Fe) had a slope of −60 mV/pH, which is indicative for deprotonation events that couple with the oxidation of the Fe complex (*4*, *8*, *9*). Our computation also shows this pH dependence in the $Q_A^0Q_B^0$ redox state (Figure 2). From discussion in the previous section, D1-Glu244 is a candidate that significantly contributes to the pH dependence of E_m-(Fe). To elucidate the origin of this pH dependence in more detail, in the present study we consider a more simplified system, in which only the D1/D2 proteins are titratable and the other PSII subunits are kept invariant in the standard protonation state.

In this model computation, we obtained a pH dependence of E_m(Fe) with a slope of −50 mV/pH in the pH range of 5−9, suggesting that most of the pH dependence originates from titratable residues in the D1/D2 complex. When the protonation state of D1-Glu244 is constrained (either to ionized or protonated) in the same model system, the pH dependence of E_m(Fe) becomes considerably smaller, exhibiting a slope of only −26 mV/pH. This implies that D1-Glu244 is significantly responsible for the pH dependence of E_m(Fe) but is not alone responsible. To suppress the pH dependence of E_m(Fe) in PSII completely, we had to increase the number of titratable residues whose protonation states are constrained and finally reached a conclusion that a cluster of titratable residues, not a single residue, is responsible for the pH dependence of E_m(Fe). These important residues are delocalized around the Fe complex in the D1/D2 unit. We obtain a relatively small pH dependence of E_m(Fe) with a slope of −17 mV/pH only when we constrain the protonation states of the following residues whose importance in the PSII protein complex was suggested formerly: five Glu residues (D1-242−244 and D2-241−242) in the D-*de* loop (*20*, 38) and six basic residues [D2-Arg233, D2-Arg251 (*39*), D1-His252 (*40*), D2-Lys264, D2-Arg265 (*35*, *41*), and D1-Arg269 (*42*, *43*)] (Figure 1). In the present study, we assign the stoichiometric proton release upon oxidation of the Fe complex largely to a few key residues, namely, (i) D1-Glu244, D1-His252, and D1-Glu243 in the $Q_A^0Q_B^0$ redox state (Figure 4a), (ii) D2-Lys264, PsbT-Arg24, D1-Glu244, and D1-His252 in the $Q_A^-Q_B^0$ redox state (Figure 4b), and (iii) D1-Glu244, D1-His252, and D1-Glu243 in the $Q_A^0Q_B^-$ redox state (Figure 4c). Nevertheless, these residues are not always coupled to the redox state of the Fe complex directly. In some cases, proton release (or uptake) is a consequence of reduction of Q_A or Q_B rather than oxidation of the Fe complex (see Figure 5).

The necessity of several titratable residues in accounting for the pH dependence of E_m(Fe) is in line with the conclusion of Berthomieu and Hienerwadel (*44*). They suggested that modeling the changes of E_m(Fe) upon bicarbonate replacement by other carboxylate anions requires a delocalized network of titratable residues (*44*). Indeed, forcing D1-Glu244 to be deprotonated invoked D1-Glu243 to be protonated as a consequence of charge compensation. Furthermore, simultaneous enforced deprotonation of both D1-Glu243 and D1-Glu244 results in protonation of D2-Glu242. These strong interactions among a cluster of Glu residues in the D-*de* loop imply that they serve as a proton network and internal proton reservoir for the Fe complex. This delocalized network of titratable residues could explain the mutant studies of Mäenpää et al. (*45*) where a single mutation of D1-Glu243 to Lys did not alter the phenotype of PSII but modulation of the ET process from Q_A^- to Q_B resulted from the deletion of three Glu (D1−242, D1−243, and D1−244). Hence, the relatively large influence of D1-Glu244 on the pH dependence of E_m(Fe) can be understood only within the frame of the proton network consisting of the residues mentioned above.

pH Dependence of E_m(Fe) in Experiment and Computation. In the experimental redox titration, the pH dependence of E_m(Fe) in PSII exhibited a slope of −60 mV/pH in the pH range of 5.5−8.5 (*4*, *8*, *9*). In the present study, the pH dependence of E_m(Fe) in the $Q_A^0Q_B^0$ redox state is −59 mV/pH at pH 5−7, which is consistent with the experimental redox titration. We obtain essentially the same pH dependence of −56 mV/pH in the $Q_A^0Q_B^-$ redox state (Figure 2). In contrast, in the $Q_A^-Q_B^0$ redox state the pH dependence of E_m(Fe) is −38 mV at pH 5−7 (Figure 2). Since the experimental pH dependence of E_m(Fe) in PSII exhibits a slope of −60 mV/pH in the pH range of 5.5−8.5 (*4*, *8*, *9*), our results suggest that a completely reduced Q_A is not relevant. In turn, this may not exclude a possibility that the Q_A^- state is more functional at pH values outside of the 5.5−8.5 interval.

In comparison of experimental and computed data, the following factors need to be considered. We calculated E_m-(Fe) in the fixed redox states of $Q_A^0Q_B^0$, $Q_A^-Q_B^0$, and $Q_A^0Q_B^-$. To compute E_m(Fe) as the "midpoint potential" of the Fe complex, we generate an equal amount of oxidized and reduced states of the Fe complex and apply the Nernst equation. However, this idealized condition may not always hold for experimental redox titration, where the redox change of the Fe complex can be accompanied also with a change in the redox state of $Q_{A/B}$. A separation of these different influences is not easy (for instance, see refs *11*, *35*, and *46*). Furthermore, heterogeneity in the oxidation event of the Fe complex has been indicated (*41*). EPR studies showed that PSII samples in the $Fe^{2+}Q_A^-$ state consist of conformers with $g = 1.82$ ($g = 1.84$ in ref *12*) and $g = 1.9$ (*47*). Among a number of BBY-PSII preparations with enrichment of the $g = 1.82$ conformer, oxidation of the Fe complex by ferricyanide was more difficult, even at pH 7 (*12*) (see also later discussion).

Another factor is the structural change of a protein associated with changes of pH or solvent redox potential. Specifically, the Fe complex of PSII is in the vicinity of the hydrophilic D-*de* loop, which is rich in titratable residues (Figure 1). In the PSII crystal structure (*15*), the Fe complex

Table 1: Protonation States (H^+) of Residues for Different $Q_{A/B}$ Redox States with an Equal Amount of [Fe^{2+}] and [Fe^{3+}] States of the Fe Complex[a] at pH 7

	protonation states[b]		
residues	$Q_A^0Q_B^0$	$Q_A^-Q_B^0$	$Q_A^0Q_B^-$
D1-Glu244	0.39	0.77	0.48
D1-His252	0.07	0.07	0.61
PsbT-Arg24	0.69	0.96	0.71

[a] For the main purpose of investigating the influence of the protonation pattern on E_m(Fe), all of the protonation states were calculated in the presence of an equal amount of [Fe^{2+}] and [Fe^{3+}] states, as E_m(Fe) is defined. [b] Fully protonated or deprotonated states were defined as protonation states with 1.0 H^+ or 0.0 H^+, respectively.

is likely to refer to the reduced state, which is energetically more stable. As shown in the present study, the protonation states of titratable residues near the Fe complex are sensitive to solvent pH and the redox state of the Fe complex (and also the redox state of $Q_{A/B}$). Therefore, oxidation of the Fe complex may be accompanied by structural changes of nearby residues as a consequence of electrostatic interactions with the negatively charged acidic residues as discussed in ref *9*. If this is the case, this could result in discrepancies between experimental and computational results, especially for the titration at pH distant from pH 7. Thus, the discrepancy in the slope of the E_m(Fe) pH dependence in low- and high-pH regions may have two possible reasons: (i) difficulties of the experimental approach to identify the E_m(Fe) to strong coupling with different $Q_{A/B}$ redox states and (ii) inability of our approach to consider possible structural changes of PSII accompanied with changes in pH and protonation states of titratable residues in the D-*de* loop.

Influence of the Q_A/Q_B Redox State on E_m(Fe). We obtained E_m(Fe) = +302 mV for the $Q_A^-Q_B^0$ state and +268 mV for the $Q_A^0Q_B^-$ state at pH 7 relative to E_m(Fe) = +400 mV for the $Q_A^0Q_B^0$ state. These results suggest that the Q_B^- state stabilizes the oxidized state of the Fe complex more effectively than the Q_A^- state. Apparently, the location of Q_A and Q_B is symmetric with respect to the Fe complex and bicarbonate (*15*). Therefore, the different influence of the two quinones on E_m(Fe) should be attributed to different arrangements of titratable residues at the Q_A/Q_B side or differences in the protonation pattern upon formation of Q_A^-/Q_B^-. For each redox state $Q_A^0Q_B^0$, $Q_A^-Q_B^0$, and $Q_A^0Q_B^-$, we calculated the protonation pattern of titratable residues in the whole PSII complex (Figure 3). The formation of negatively charged Q_A^- results in increased protonation by 0.4 H^+ at D1-Glu244 and by 0.3 H^+ at PsbT-Arg24 (Table 1). The latter is a residue outside of the D1/D2 proteins but relatively close to Q_A ($O_{QA}-N_{Arg}$ distance of 6.6 Å) (Figure 1). Protonation states of these two residues remain unaffected by formation of Q_B^-; i.e., D1-Glu244 remains deprotonated and PsbT-Arg24 partially deprotonated. On the other hand, D1-His252 becomes more protonated by 0.5 H^+ (Table 1) upon formation of Q_B^-. This resembles a proton uptake ability of Glu-L212 in bRC from *Rhodobacter sphaeroides* observed in previous computations (*48*−*50*) (for further details, see the next section).

Since D1-Glu244 is the acidic residue that is closest to the bicarbonate (∼5 Å) and the Fe complex (∼9 Å from Fe) (*15*), obviously, the protonation state of D1-Glu244 has a direct impact on the redox behavior of the Fe complex and vice versa. According to the crystal structure (*15*), Q_B is via D1-Ser264 involved in an H-bond network with D1-His252 (Figure 1). This Q_B H-bond network facilitates protonation of the remote, solvent-exposed D1-His252 upon formation of Q_B^- as a consequence of charge compensation. In this case, D1-Glu244 does not have to protonate. The solvent exposure of D1-His252 and its relatively large distance from the Fe complex (∼14 Å from Fe) diminish its direct electrostatic influence on E_m(Fe). On the other hand, such an H-bond network extending over ∼14 Å is absent in the Q_A side of PSII. Therefore, to compensate the negative charge on Q_A^-, PSII has only the possibility to react with protonation of D1-Glu244. Due to the proximity of D1-Glu244 to the Fe complex (∼9 Å from Fe), protonation at D1-Glu244 upshifts E_m(Fe) considerably as compared to a protonation of the more distant D1-His252.

Light-Induced Oxidation of the Fe Complex by Exogenous Q_B. Zimmermann and Rutherford (*11*) found that, after reconstituting high-potential exogenous quinone at the Q_B site (for instance, by phenyl-*p*-benzoquinone), light-induced oxidation of the Fe complex could be observed without support of ferricyanide. Later, Petrouleas and Diner also observed reversible oxidation of the Fe complex by similar exogenous Q_B (*12*, *17*). It also has been established that inhibition of ET from Q_A^- to Q_B by DCMU, a herbicide, results in inhibition of Fe complex oxidation by ferricyanide (*4*). On the basis of these facts, Petrouleas and Diner proposed the following sequential reactions (*12*); (i) in the first flash, ET from Q_A^- to Q_B occurs in the Fe^{2+} state and leads to the formation of the $Q_A^0Fe^{2+}Q_B^-$ state. The ET from Fe^{2+} to Q_B^- coupled to net protonation of Q_B by two H^+ results in $Q_A^0Fe^{3+}Q_BH_2$; (ii) in the second flash, ET from Q_A^- to Fe^{3+} completes the $Q_A^0Fe^{2+}Q_BH_2$ state (*12*).

Indeed, the $E_m(Q^-/QH_2)$ of +573 mV for phenyl-*p*-benzoquinone (*11*) would be high enough to reduce the oxidized Fe complex (in step ii). However, the value of $E_m(Q^-/QH_2)$ cannot fully explain the efficiency to form $Fe^{3+}Q_BH_2$ with respect to the $E_m(Q^-/QH_2)$ for other exogenous quinones, implying involvement of other factors (*11*). From this viewpoint, one may argue about differences in binding affinity of these exogenous quinones in the Q_B binding site (*17*). In addition, in previous computations for bRC (*51*, *52*) it was also demonstrated that formation of Q_BH_2 proceeds energetically more favorably via Q_BH and Q_BH^- rather than via the direct double protonation of Q_B^-. Therefore, we assume that formation of $Fe^{3+}Q_BH_2$ in PSII occurs via the intermediate states of Q_BH and Q_BH^-. The involvement of these intermediate states in the net reaction does not change the stoichiometry of the net reaction of one electron and two protons, in which the net pH dependence for $Fe^{3+}Q_BH_2$ formation remains −60 mV/pH.

We consider that, to enable this ET from Fe^{2+} to Q_B, besides a high-potential quinone protonation of D1-His252 is probably important to upshift the $E_m(Q_B)$, making Q_B energetically more suitable as an electron acceptor. The lack of such an H-bond network in the Q_A side makes it more difficult for PSII to recruit other distant titratable residues besides D1-Glu244 to stabilize the negatively charged Q_A^-. Here we propose that proton release from D1-His252 is related to the efficiency of the Fe complex oxidation. Upon

the $Fe^{2+}Q_B^- \rightarrow Fe^{3+}Q_B^{uncharged}$ reaction, we observe significant proton release from D1-His252 at pH 5−8 (Figure 4e). Note that $Q_B^{uncharged}$ stands for the states Q_B^0, Q_BH^0, and $Q_BH_2^0$. Zimmermann and Rutherford observed that at pH 5.5 light-induced oxidation of the Fe complex by exogenous Q_B^- was drastically decreased to a yield of 20% (*11*). In this connection, Wraight reported the occurrence of an apparent $pK_{Fe(oxidized)}$ at 5.3 and the absence of proton release below pH 5 (*9*). Consistent with these experimental findings, we observed in our computations a significant decrease of proton release from D1-His252 below pH 5 (Figure 4e) where D1-His252 is strongly protonated for the reduced and oxidized Fe complex. Furthermore, we obtain maximum proton release from D1-His252 at pH 6−7 (Figure 4e). Indeed, Petrouleas and Diner obtained maximum efficiency of the formation of $Fe^{3+}Q_BH_2$ in the same pH range of 6−7 (*12*), which is considered as the typical physiological pK_a for His.

D1-His252 is a residue near the Q_B binding site (Figure 1). Proton uptake (Table 1) and release (Figure 4e) at D1-His252 resemble a proton uptake ability of Glu-L212 in bRC from *Rhodobacter sphaeroides* observed in previous computations (*48*−*50*). According to sequence alignment [based on analysis with CLUSTAL (*53*)], Glu-L212 in bRC is replaced by Ala in PSII, but the next residue Asp-L213 in bRC corresponds to D1-His252 in PSII. Since the protonation state of Asp-L213 directly affects the H-bond pattern for Q_B (*50*, *52*, *54*, *55*), proton uptake of D1-His252 in PSII could be interpreted in analogy to protonation of Glu-L212/Asp-L213 in bRC. In bRC, the proton needed to form Q_BH from Q_B^- is transferred via Ser-L223 to the distal carbonyl oxygen of Q_B (reviewed in refs *22* and *51*). Ser-L223 in bRC corresponds to D1-Ser264 in PSII (Figure 1). D1-His252 is in H-bond distance to D1-Ser264. Hence, loss of proton release from D1-His252 at low pH may result in inefficient Q_B^- protonation. Neutralization of the negatively charged Q_B^- by proton release from D1-His252 should be coupled to or even be a prerequisite for efficient Fe complex oxidation. Otherwise, Fe^{2+} should be oxidized to Fe^{3+} simultaneously with electron donation to the negatively charged Q_B^- [i.e., corresponding to $E_m(Q_B^-/Q_B^{2-})$], which is energetically very unfavorable.

EPR Signals at g = 1.82 and g = 1.9 Relate to the Ability of D1-His252 To Deprotonate or Not. EPR studies showed that PSII samples in the $Fe^{2+}Q_A^-$ state consist of conformers with $g = 1.82$ (1.84 in ref *12*) or $g = 1.9$ (*47*). Rutherford and Zimmermann proposed that the two forms of the $Fe^{2+}Q_A^-$ state ($g = 1.82$ and $g = 1.9$ conformers) reflect different protonation states of a titratable residue near the Fe complex or $Q_{A/B}$, since (i) lowering the pH resulted in a population increase of the PSII conformer with $g = 1.82$ at the expense of that with $g = 1.9$ and (ii) an apparent pK_a of 7−8 obtained from the ratio of the two conformers excluded a direct protonation event of Q_B (*47*).

Petrouleas and Diner demonstrated that it was more difficult to oxidize the Fe complex of PSII in the $g = 1.82$ conformer than in the $g = 1.9$ conformer (*12*). As discussed in the present study (see also Figure 4e), proton release from D1-His252 could be necessary for efficient $Fe^{3+}Q_BH_2$ formation. At low pH, D1-His252 is not able to release a proton due to its persistent protonation for the reduced and oxidized Fe complex. Due to a number of remarkable features consistent with experimental results, the protonation behavior of D1-His252 observed in the present study is an indication that the EPR signals at $g = 1.82$ and $g = 1.9$ can be attributed to two different D1-His252 populations, the former being capable of releasing a proton and the latter not. Indeed, addition of the phenolic herbicide DINOSEB at pH 8.5 resulted in an increased population of the $g = 1.82$ conformer, indicating that the titratable residue responsible for the $g = 1.82$ and $g = 1.9$ conformers should be a key residue associated with ET between Q_A and Q_B (*47*). Therefore, Rutherford and Zimmermann proposed that this titratable residue is the same residue that is responsible for proton uptake upon formation of the Q_B^- state (*47*), which is in agreement with our assignment of D1-His252 to the origin of the $g = 1.82$ and $g = 1.9$ conformers.

The involvement of a His residue near Q_B in oxidation of the Fe complex was also suggested by FTIR studies of Berthomieu and Hienerwadel (*13*, *44*). They observed a stoichiometric one-proton release from a His residue upon oxidation of the Fe complex by ferricyanide. Although their measurements did not refer to PSII samples reconstituted with high-potential exogenous quinones, we assume that D1-His252 could also contribute to proton release under these conditions as observed in the FTIR studies.

In the previous part, we referred to D1-Glu244 as one of the titratable residues responsible for variation of the pK_a with the Fe complex redox state, discussed by Wraight (*9*) or Deligiannakis et al. (*35*, *36*). However, an uncertainty remains in the interpretation of experimental redox titrations, because the redox change of the Fe complex is accompanied with that of $Q_{A/B}$ (*11*, *35*, *46*) (see discussion in previous part). This may include the case where the oxidation of the Fe complex is coupled to the Q_B redox state discussed here. In this case, D1-His252 can also be the titratable residue.

On the other hand, D1-His252 is obviously more distant from the bicarbonate binding site than D1-Glu244 (Figure 1). As discussed in the present study, both D1-Glu244 and D1-His252 are in the same network of residues serving as an internal proton reservoir. Therefore, we assume that both of the two residues are, more or less, related to the titratable residue discussed by Wraight (*9*) or Deligiannakis et al. (*35*, *36*). It might well be that the residue of Wraight (*9*) and that of Deligiannakis et al. (*35*, *36*) are identical. Nevertheless, it should again be noted that the titratable residue discussed by Deligiannakis et al. (*35*, *36*) refers to the one whose pK_a was affected by the bicarbonate replacement. This background of their original suggestion can be indicative of a residue, not necessarily but preferentially, located close to the bicarbonate binding site. At this point, we consider that D1-Glu244 is more likely the titratable residue proposed by Deligiannakis et al. (*35*, *36*), possibly together with other titratable residues in the D-*de* loop.

Protonation State of the PsbT Protein in Response to Q_A/Fe Redox Change. The change in protonation of PsbT-Arg24 with a change of the Fe complex redox state observed in the present study is somewhat unexpected, since this residue is at a distance of ∼17 Å from the iron of the Fe complex. On the other hand, PsbT-Arg24 is relatively close to Q_A. Its basic guanidinium group is at a distance of only 6.6 Å from the Q_A carbonyl oxygen (Figure 1). Therefore, this basic residue, which is highly conserved in the PsbT protein, changes its protonation also with the redox state of Q_A.

It was suggested that the PsbT protein might not be essential for stability and function of PSII (*56*), since the *psbT* lacking mutant in *Chlamydomonas reinhardtii* resulted in only slightly impaired PSII activity with respect to the wild-type PSII. On the other hand, recent studies suggested that under strong illumination PSII activity was reduced in the *psbT* lacking mutant more significantly than that in wild-type PSII (*57*). It was therefore concluded that PsbT may not be relevant for photoprotection but important for an efficient recovery of photodamaged PSII (*57*). Thus, proximity and protonation state coupling of PsbT-Arg24 with the Q_A redox state have a potential importance for the mechanism of recovering photoinhibited PSII. Although our present data do not provide further information on this issue except for protonation at PsbT-Arg24 upon formation of Q_A^-, it may be speculative that PsbT-Arg24 is responsible for a proton uptake event related to Q_A, for instance, removing protons from protonated Q_A, a possible product of photoinhibited PSII.

CONCLUDING REMARKS

In the $Q_A^0Q_B^0$ redox state, the protonation state of D1-Glu244 is significantly coupled to the oxidation state of the Fe complex. However, to account for the pH dependence of the calculated E_m(Fe), other residues, at least D1-Glu243, D1-His252, D2-Lys264, D2-Arg265, and PsbT-Arg24, need to be considered. The coupling of these residues to the redox state of the Fe complex varies significantly in the different $Q_{A/B}$ redox states and at different pH, implying the existence of a network of residues in the D-*de* loop serving as an internal proton reservoir. Upon formation of the $Q_A^-Q_B^0$ or $Q_A^-Q_B^0$ redox states, E_m(Fe) is downshifted significantly. Especially, protonation of D1-His252 in the $Q_A^0Q_B^-$ redox state, presumably via an H-bond network involving D1-Ser264, plays an important role in stabilizing the oxidized state of the Fe complex, resulting in downshift of E_m(Fe). Upon the $Fe^{2+}Q_B^- \rightarrow Fe^{3+}Q_B^{uncharged}$ ET reaction, which was suggested to occur photochemically in PSII after the reconstitution of native Q_B with high-potential exogenous quinone, we observed significant proton release from D1-His252. The degree of proton release from D1-His252 going along with this redox reaction relates to the oxidation efficiency of the Fe complex observed in experimental studies. We conclude that neutralization of the negatively charged Q_B^- by a proton released from D1-His252 should be coupled to or even a prerequisite for efficient oxidation of the Fe complex. Thus, it is likely that EPR signals for the $Fe^{2+}Q_A^-$ state at $g = 1.82$ and $g = 1.9$ can be attributed to two different protonation states of D1-His252, the former being capable of releasing a proton and the latter not. Therefore, the titratable residue discussed by Wraight (*9*) can be D1-His252, especially when the oxidation of the Fe complex is associated with a redox change of Q_B. On the other hand, Deligiannakis et al. (*35*, *36*) suggested that a residue whose pK_a is affected by bicarbonate replacement should directly influence the redox behavior of the Fe complex. We suggest that D1-Glu244 could play this role, possibly together with other titratable residues in the D-*de* loop.

ACKNOWLEDGMENT

We thank Dr. Donald Bashford and Dr. Martin Karplus for providing the programs MEAD and CHARMM22, respectively. We also thank Dr. Wolfram Saenger, Dr. Jacek Biesiadka, and Dr. Bernhard Loll for useful discussions.

SUPPORTING INFORMATION AVAILABLE

One table listing the atomic partial charge of the Fe complex. This material is available free of charge via the Internet at http://pubs.acs.org.

REFERENCES

1. Michel, H., and Deisenhofer, J. (1988) Relevance of the photosynthetic reaction center from purple bacteria to the structure of photosystem II, *Biochemistry 27*, 1−7.
2. Debus, R. J., Feher, G., and Okamura, M. Y. (1986) Iron-depleted reaction centers from *Rhodopseudomonas sphaeroides* R-26.1: characterization and reconstitution with Fe^{2+}, Mn^{2+}, Co^{2+}, Ni^{2+}, Cu^{2+}, and Zn^{2+}, *Biochemistry 25*, 2276−2287.
3. Remy, A., and Gerwert, K. (2003) Coupling of light-induced electron transfer to proton uptake in photosynthesis, *Nat. Struct. Biol. 10*, 637−644.
4. Petrouleas, V., and Diner, B. A. (1986) Identification of Q_{400}, a high-potential electron acceptor of photosystem II, with the iron of the quinone-iron acceptor complex, *Biochim. Biophys. Acta 849*, 264−275.
5. Stemler, A., and Murphy, J. B. (1985) Determination of the binding constant of $H^{14}CO_3^-$ to the photosystem II complex in maize chloroplasts: effects of inhibitors and light, *Plant Physiol. 77*, 974−977.
6. van Rensen, J. J. S., Tonk, W. J. M., and de Bruijn, S. M. (1988) Involvement of bicarbonate in the protonation of the secondary quinone electron acceptor of photosystem II via the non-haem iron of the quinone-iron acceptor complex, *FEBS Lett. 226*, 347−351.
7. Koulougliotis, D., Kostopoulos, T., Petrouleas, V., and Diner, B. A. (1993) Evidence for CN^- binding at the PSII non-heme Fe^{2+}. Effects on the EPR signal for $Q_A^-Fe^{2+}$ and on Q_A/Q_B electron transfer, *Biochim. Biophys. Acta 1141*, 275−282.
8. Bowes, J. M., Crofts, A. R., and Itoh, S. (1979) A high potential acceptor for photosystem II, *Biochim. Biophys. Acta 547*, 320−335.
9. Wraight, C. A. (1985) Modulation of herbicide-binding by the redox state of Q_{400}, an endogenous component of photosystem II, *Biochim. Biophys. Acta 809*, 320−330.
10. Nugent, J. H. A. (1996) Oxygenic photosynthesis, *Eur. J. Biochem. 237*, 519−531.
11. Zimmermann, J.-L., and Rutherford, A. W. (1986) Photoreductant-induced oxidation of Fe^{2+} in the electron-acceptor complex of photosystem II, *Biochim. Biophys. Acta 851*, 416−423.
12. Petrouleas, V., and Diner, B. A. (1987) Light-induced oxidation of the acceptor-side Fe(II) of photosystem II by exogenous quinones acting through the Q_B binding site. I. Quinones, kinetics and pH-dependence, *Biochim. Biophys. Acta 893*, 126−137.
13. Hinerwadel, R., and Berthomieu, C. (1995) Bicarbonate binding to the non-heme iron of photosystem II investigated by Fourier transform infrared difference spectroscopy and ^{13}C-labeled bicarbonate, *Biochemistry 34*, 16288−16297.
14. Nugent, J. H. A., Corrie, A. R., Demetriou, C., Evans, M. C. W., and Lockett, C. J. (1988) Bicarbonate binding and the properties of photosystem II electron acceptors, *FEBS Lett. 235*, 71−75.
15. Ferreira, K. N., Iverson, T. M., Maghlaoui, K., Barber, J., and Iwata, S. (2004) Architecture of the photosynthetic oxygen-evolving center, *Science 303*, 1831−1838.
16. Berthold, D. A., Babcock, G. T., and Yocum, C. F. (1981) A highly resolved, oxygen-evolving photosystem II preparation from spinach thylakoid membranes: EPR and electron-transport properties, *FEBS Lett. 134*, 231−234.
17. Diner, B. A., and Petrouleas, V. (1987) Light-induced oxidation of the acceptor-side Fe(II) of photosystem II by exogenous quinones acting through the Q_B binding site. II. Blockage by inhibitors and their effects on the Fe(III) EPR spectra, *Biochim. Biophys. Acta 893*, 138−148.

18. Remy, A., Niklas, J., Kuhl, H., Kellers, P., Schott, T., Rögner, M., and Gerwert, K. (2004) FTIR spectroscopy shows structural similarities between photosystems II from cyanobacteria and spinach, *Eur. J. Biochem. 271*, 563−567.
19. Deisenhofer, J., Epp, O., Miki, K., Huber, R., and Michel, H. (1985) Structure of the protein subunits in the photosynthetic reaction centre of *Rhodopseudomonas viridis* at 3 Å resolution, *Nature 318*, 618−624.
20. Greenberg, B. M., Gaber, V., Mattoo, A. K., and Edelman, M. (1987) Identification of a primary in vivo degradation product of the rapidly turning over 32 Kd protein of photosystem II, *EMBO J. 6*, 2865−2869.
21. Sebban, P., Maróti, P., Schiffer, M., and Hanson, D. K. (1995) Electrostatic dominoes: long distance propagation of mutational effects in photosynthetic reaction centers of *Rhodobacter capsulatus*, *Biochemistry 34*, 8390−8397.
22. Okamura, M. Y., Paddock, M. L., Graige, M. S., and Feher, G. (2000) Proton and electron transfer in bacterial reaction centers, *Biochim. Biophys. Acta 1458*, 148−163.
23. Brooks, B. R., Bruccoleri, R. E., Olafson, B. D., States, D. J., Swaminathan, S., and Karplus, M. (1983) CHARMM: a program for macromolecular energy minimization and dynamics calculations, *J. Comput. Chem. 4*, 187−217.
24. MacKerell, A. D., Jr., Bashford, D., Bellott, R. L., Dunbrack, R. L., Jr., Evanseck, J. D., Field, M. J., Fischer, S., Gao, J., Guo, H., Ha, S., Joseph-McCarthy, D., Kuchnir, L., Kuczera, K., Lau, F. T. K., Mattos, C., Michnick, S., Ngo, T., Nguyen, D. T., Prodhom, B., Reiher, W. E., III, Roux, B., Schlenkrich, M., Smith, J. C., Stote, R., Straub, J., Watanabe, M., Wiorkiewicz-Kuczera, J., Yin, D., and Karplus, M. (1998) All-atom empirical potential for molecular modeling and dynamics studies of proteins, *J. Phys. Chem. B 102*, 3586−3616.
25. Rabenstein, B., Ullmann, G. M., and Knapp, E. W. (1998) Calculation of protonation patterns in proteins with structural relaxation and molecular ensembles—application to the photosynthetic reaction center, *Eur. Bophys. J. 27*, 626−637.
26. Ishikita, H., and Knapp, E. W. (2005) Redox potentials of chlorophylls and β-carotene in the antenna complexes of photosystem II, *J. Am. Chem. Soc. 127*, 1963−1968.
27. Ishikita, H., Loll, B., Biesiadka, J., Saenger, W., and Knapp, E. W. (2005) Redox potentials of chlorophylls in the photosystem II reaction center, *Biochemistry 44*, 4118−4124.
28. Ishikita, H., and Knapp, E. W. (2005) Redox potential of cytochrome *c*550 in the cyanobacterium *Thermosynechococcus elongatus*, *FEBS Lett. 579*, 3190−3194.
29. Bayly, C. I., Cieplak, P., Cornell, W. D., and Kollman, P. A. (1993) A well-behaved electrostatic potential based method using charge restraints for deriving atomic charges: the RESP model, *J. Phys. Chem. 97*, 10269−10280.
30. Jaguar4.2 (1991−2000) Schrödinger, Inc., Portland, OR.
31. Yachandra, V. K., Sauer, K., and Klein, M. P. (1996) Manganese cluster in photosynthesis: where plants oxidize water to dioxygen, *Chem. Rev. 96*, 2927−2950.
32. Bashford, D., and Karplus, M. (1990) pK_a's of ionizable groups in proteins: atomic detail from a continuum electrostatic model, *Biochemistry 29*, 10219−10225.
33. Rabenstein, B. (1999) *Karlsberg online manual* (http://agknapp.chemie.fu-berlin.de/karlsberg/).
34. Ishikita, H., and Knapp, E. W. (2005) Energetics of proton transfer pathways in reaction centers from *Rhodobacter sphaeroides*: the Glu-H173 activated mutants, *J. Biol. Chem. 280*, 12446−12450.
35. Deligiannakis, Y., Petrouleas, V., and Diner, B. A. (1994) Binding of carboxylate anions at the non-heme Fe(II) of PSII. I. Effects on the $Q_A^-Fe^{2+}$ and Q_AFe^{3+} EPR spectra and the redox properties of the iron, *Biochim. Biophys. Acta 1188*, 260−270.
36. Petrouleas, V., Deligiannakis, Y., and Diner, B. A. (1994) Binding of carboxylate anions at the non-heme Fe(II) of PSII. II. Competition with bicarbonate and effects on the Q_A/Q_B electron transfer rate, *Biochim. Biophys. Acta 1188*, 271−277.
37. Mulo, P., Tyystjärvi, T., Tyystjärvi, E., Govindjee, Mäenpää, P., and Aro, E.-M. (1997) Mutagenesis of the D-E loop of photosystem II reaction centre protein D1. Function and assembly of photosystem II, *Plant Mol. Biol. 33*, 1059−1071.
38. Shipton, C. A., Marder, J. B., and Barber, J. (1989) Determination of catabolism of the photosystem II D1 subunit by structural motifs in the polypeptide sequence, *Z. Naturforsch. 45C*, 388−394.
39. Cao, J. C., Vermaas, W. F. J., and Govindjee (1991) Arginine residues in the D2 polypeptide may stabilize bicarbonate binding in photosystem II of *Synechocystis* sp. PCC, *Biochim. Biophys. Acta 1059*, 171−180.
40. Sigfridsson, K. G. V., Bernat, B., Mamedov, F., and Styring, S. (2004) Molecular interference of Cd^{2+} with photosystem II, *Biochim. Biophys. Acta 1659*, 19−31.
41. Diner, B. A., Petrouleas, V., and Wendoloski, J. J. (1991) The iron-quinone electron-acceptor complex of photosystem II, *Physiol. Plant. 81*, 423−436.
42. Hutchison, R. S., Xiong, J., Sayre, R. T., and Govindjee. (1996) Construction and characterization of a photosystem II D1 mutant (arginine-269-glycine) of *Chlamydomonas reinhardtii*, *Biochim. Biophys. Acta 1277*, 83−92.
43. Xiong, J., Hutchison, R. S., Sayre, R. T., and Govindjee (1997) Modification of the photosystem II acceptor side function in a D1 mutant (arginine-269-glycine) of *Chlamydomonas reinhardtii*, *Biochim. Biophys. Acta 1322*, 60−76.
44. Berthomieu, C., and Hienerwadel, R. (2001) Iron coordination in photosystem II: Interaction between bicarbonate and the Q_B pocket studied by Fourier transform infrared spectroscopy, *Biochemistry 40*, 4044−4052.
45. Mäenpää, P., Miranda, T., Tyystjärvi, E., Tyystjärvi, T., Govindjee, Ducruet, J. M., Etienne, A. L., and Kirilovsky, D. (1995) A mutation in the D-de loop of D_1 modifies the stability of the $S_2Q_A^-$ and $S_2Q_B^-$ states in photosystem II, *Plant Physiol. 107*, 187−197.
46. Hallahan, B. J., Ruffle, S. V., Bowden, S. J., and Nugent, J. H. A. (1991) Identification and characterisation of EPR signals involving Q_B semiquinone in plant photosystem II, *Biochim. Biophys. Acta 1059*, 181−188.
47. Rutherford, A. W., and Zimmermann, J.-L. (1984) A new EPR signal attributed to the primary plastosemiquinone acceptor in photosystem II, *Biochim. Biophys. Acta 767*, 168−175.
48. Rabenstein, B., Ullmann, G. M., and Knapp, E. W. (2000) Electron transfer between the quinones in the photosynthetic reaction center and its coupling to conformational changes, *Biochemistry 39*, 10487−10496.
49. Ishikita, H., Morra, G., and Knapp, E. W. (2003) Redox potential of quinones in photosynthetic reaction centers from *Rhodobacter sphaeroides*: dependence on protonation of Glu-L212 and Asp-L213, *Biochemistry 42*, 3882−3892.
50. Ishikita, H., and Knapp, E. W. (2004) Variation of Ser-L223 hydrogen bonding with the Q_B redox state in reaction centers from *Rhodobacter sphaeroides*, *J. Am. Chem. Soc. 126*, 8059−8064.
51. Rabenstein, B., Ullmann, G. M., and Knapp, E. W. (1998) Energetics of electron-transfer and protonation reactions of the quinones in the photosynthetic reaction center of *Rhodopseudomonas viridis*, *Biochemistry 37*, 2488−2495.
52. Zhu, Z., and Gunner, M. R. (2005) Energetics of quinone-dependent electron and proton transfers in *Rhodobacter sphaeroides* photosynthetic reaction centers, *Biochemistry 44*, 82−96.
53. Higgins, D. G., Thompson, J. D., and Gibson, T. J. (1996) Using CLUSTAL for multiple sequence alignments, *Methods Enzymol. 266*, 383−402.
54. Alexov, E. G., and Gunner, M. R. (1999) Calculated protein and proton motions coupled to electron transfer: electron transfer from Q_A^- to Q_B in bacterial photosynthetic reaction centers, *Biochemistry 38*, 8253−8270.
55. Paddock, M. L., Flores, M., Isaacson, R., Chang, C., Selvaduray, P., Feher, G., and Okamura, M. Y. (2005) Hydrogen bond reorientation upon Q_B reduction revealed by ENDOR spectroscopy in reaction centers from *Rhodobacter sphaeroides*, *Biophys. J. 88*, 204A.
56. Monod, C., Takahashi, Y., Goldschmidt-Clermont, M., and Rochaix, J. D. (1994) The chloroplast *ycf8* open reading frame encodes a photosystem II polypeptide which maintains photosynthetic activity under adverse growth conditions, *EMBO J. 13*, 2724−2754.
57. Ohnishi, N., and Takahashi, Y. (2001) PsbT polypeptide is required for efficient repair of photodamaged photosystem II reaction center, *J. Biol. Chem. 276*, 33798−33804.

BI051099V